Numerical study of the fracture behavior of an electron beam welded steel joint by cohesive zone modeling

Haoyun Tu*, Siegfried Schmauder, Ulrich Weber

Institute for Materials Testing, Materials Science and Strength of Materials (IMWF) University of Stuttgart, Pfaffenwaldring 32, D-70569 Stuttgart, Germany
* Corresponding author: haoyun.tu@imwf.uni-stuttgart.de

Abstract The cohesive model has been used studying the ductile and brittle fracture mechanisms of homogenous and inhomogeneous structures in recent years. The traction-separation law which is described by the cohesive strength T_0, critical separation δ_0 and cohesive energy Γ_0 is used to study the damage of materials. In this paper, the cohesive model is adopted to study the fracture behavior of an electron beam welded steel joint. The dimensions of different weld regions can be obtained from hardness tests across the welded joint. Local stress-strain curves are derived from the tensile test results of flat specimens which are obtained from the respective weld regions. Based on the axial stress versus diameter reduction curve of notched round specimens, the cohesive strength can be fixed. For pure mode I loading, the Γ_0 value is set equal to the J_i value which is the J-integral value at fracture initiation. The cohesive parameters obtained from the base material (BM), the fusion zone (FZ) and the heat affected zone (HAZ), respectively, are used to predict the fracture behavior of compact tension (C(T)) specimens with the initial crack located at different positions in the weld region. Good comparison is obtained between the numerical and the experimental results in terms of force vs. Crack Opening Displacement (COD) curves as well as fracture resistance (J_R) curves.

Keywords Cohesive zone model, electron beam welded joints, crack propagation, finite element modeling

1. Introduction

Compared to the traditional arc welding technique, advanced welding technique, such as electron beam welding (EBW) has found wide applications in industry fields as a narrow heat affected zone and small residual stresses are obtained after the welding process. The failure of the weldments always draws attentions as the fracture behavior of the welded joints influences the crack growth of structures, which affects the lifetime and safety of components. With the development of the finite element method, attention has been focused on the fracture behavior of welded joints in a numerical way. The Gurson-Tvergaard-Needlemann (GTN) model [1-3] has been used in studies of the fracture behavior of conventional fusion welded joints [4-6] and laser welded joints [7-9]. Later, the GTN model and the Rousselier model [10] were used successfully to study the ductile fracture of electron beam welded steel joints at IMWF [11-13].

Compared to the previous two damage models, the cohesive model possesses less model parameters, which make the model easy to use. The material separation is usually described by interface elements - the cohesive element, continuous elements remain undamaged in the cohesive model. The damage of the cohesive zone is depicted by a traction-separation law which is described by cohesive strength T_0, critical separation δ_0 and cohesive energy Γ_0. The concept of a cohesive model was first introduced by Dugdale [14] and Barenblatt [15]. They assume that the crack consists of two parts: the stress-free part and the parts loaded by cohesive stresses. Following this assumption, different traction-separation laws were proposed in the past to investigate the ductile or brittle

fracture behavior of a number of materials. Some typical traction-separation laws are shown in the following. The linear decreasing traction-separation law shown in Fig. 1(a) was introduced by Hillerborg [16] to describe the brittle fracture behavior of a concrete beam. The polynomial and the exponential traction-separation laws shown in Fig. 1(b-c) were provided by Needleman [17, 18] to describe the decohesion behavior. Tvergaard and Hutchinson [19] invented a trapezoid shape to study the ductile fracture of solid, this traction-separation law was later modified by Scheider [20] for the investigation of a laser welded joint. In this paper, the cohesive zone model is adopted to study fracture of S355 EBW joints.

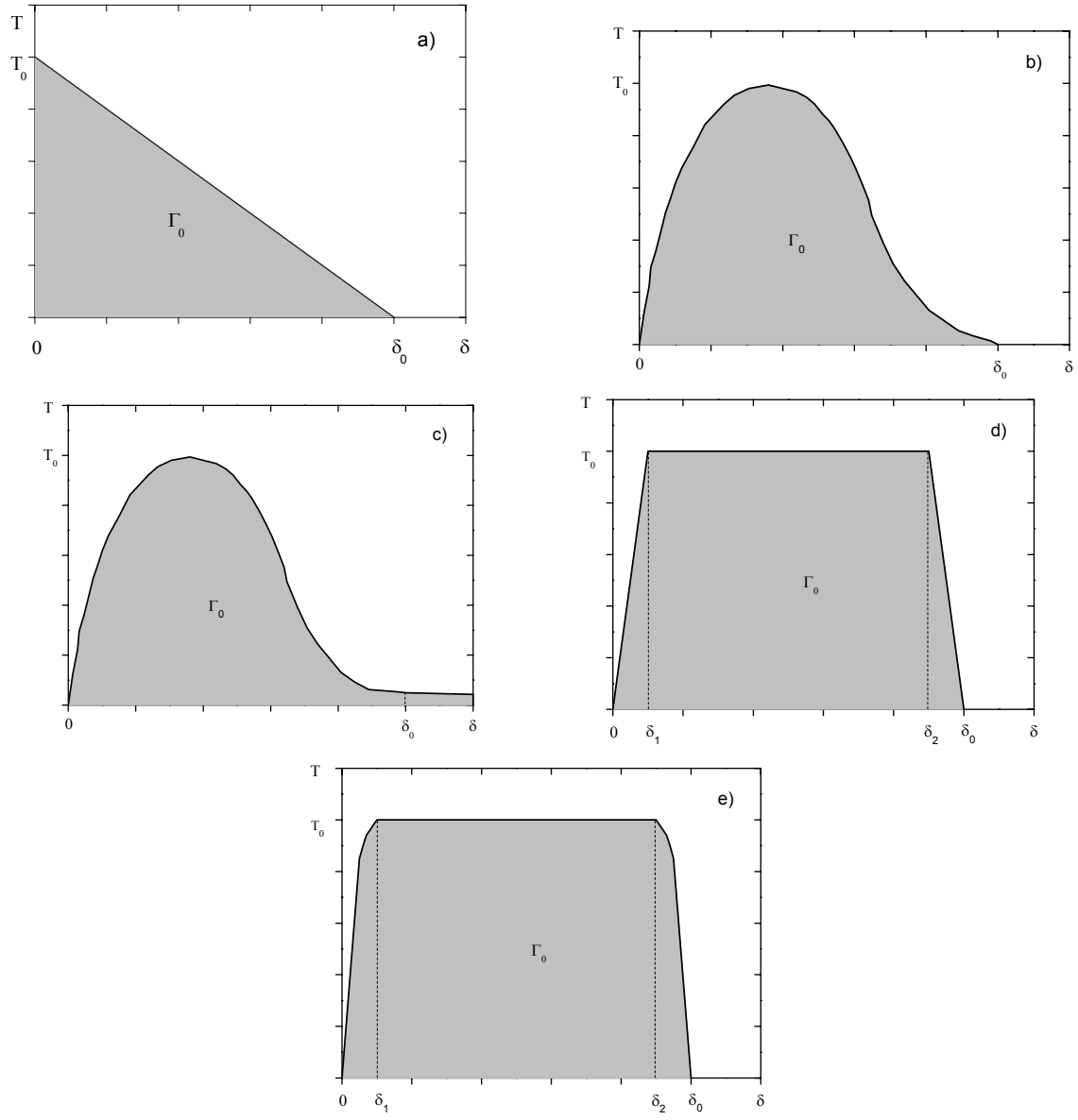

Fig. 1: Shape of traction separation laws: a) from Hillerborg [16], b)+c) from Needleman [17, 18], d) from Tvergaard and Hutchinson [19] and e) from Scheider [20] where T_0 is cohesive strength, δ_0 is critical separation and Γ_0 is cohesive energy.

2. Experimental investigations

In this paper, a low-alloyed structural steel S355NL was adopted as the base material (BM) for producing the weldments. After the electron beam welding process, a butt joint is obtained from two S355NL plates with the thickness of 60 mm. The chemical components of S355NL are shown in Table 1, which is obtained from spectrometric analysis.

Table 1: Chemical composition of the steel S355NL, mass contents in %

Steel	C	Si	Mn	P	S	Cr	Mo	Ni	Al	Co
S355NL	0.198	0.260	1.386	0.026	0.013	0.020	<0.005	<0.005	0.013	0.006

After the hardness test, the dimensions of the fusion zone (FZ) and the heat affected zone (HAZ) are found to be 2.8 mm and 3.1 mm, respectively. The mechanical properties of different weld regions of S355 EBW joints are obtained from flat specimens along the weld line of which the gauge length is 50 mm. These stress-strain curves [12] are used as finite element model input data. Table 2 shows the mechanical properties of base material (BM) and fusion zone (FZ) of the welded joints containing yield strength R_e, tensile strength R_m, uniform elongation A_g and strain at rupture A.

Table 2: Mechanical properties of different weld regions of S355NL EBW joint

R_e^{BM} (MPa)	R_e^{FZ} (MPa)	R_m^{BM} (MPa)	R_m^{FZ} (MPa)	A_g^{BM}	A_g^{FZ}	A^{BM}	A^{FZ}
348	513	533	687	0.151	0.037	0.246	0.052

Fracture toughness tests of S355 electron beam welded joints were performed using compact tension (C(T)) specimens. The specimens were manufactured and tensile tested according to ASTM standard [21] which have a thickness of B=25 mm, a net thickness of B_n=20 mm due to 20% side grooves, the width of specimen is W=50 mm. After the C(T) test, the experimental results are shown in terms of force vs. Crack Opening Displacement (COD) as well as fracture resistance J_R curves. The F-COD curves of compact tension (C(T)) specimens with initial crack located in the BM (C(T)-BM), in the center of FZ (C(T)-FZ) and at the interface between the FZ and HAZ (C(T)-HAZ) can be found in Fig. 2(a). For a C(T) specimen with the crack in the FZ, the specimen suddenly ruptures, showing a rather brittle fracture behavior. The C(T)-FZ specimen broke suddenly without stable crack propagation, no fracture resistance (J_R) curves were obtained during the test process. The J_R curves for a C(T)-BM and a C(T)-HAZ specimen can be found in Fig. 2(b).

3. Numerical calculation

Before the application, the cohesive parameters must be fixed first. According to the discussion of Cornec and Scheider [22], for mode I situation, the cohesive parameter T_0 is equal to the projection of the applied force on a plane perpendicular to the specimen cross section. The notched round specimen extracted from the BM is used for the determination of T_0. For the notched round specimen, as the geometry and loading are axisymmetric and symmetric to the cross section, only one quarter of the structure is used for the modeling. The finite element (FE) mesh of the notched round specimen and the detailed mesh can be found in Fig. 3. The comparison of axial stress versus the diameter reduction curve from the FE simulation and the experiment as well as the maximum true axial stress in the center of the specimen can be found in Fig. 4. The simulated axial stress

versus the diameter reduction curve coincides with the experimental one until crack initiation, where the experimental curve drops suddenly. At this point, the maximum value of stress distribution over the cross section of the specimen is determined from the simulation and set equal to the cohesive stress T_0. After the comparison of simulation and experiment for the BM, T_0=1180 MPa was found. The exponential and trapezoid traction-separation laws are used to study the fracture behavior of the C(T)-BM specimen. Because the structure shows symmetry with respect to the crack plane, only half of the C(T)-BM specimen is modeled, loading is defined on the loading point (Red point) by the displacement, the finite element mesh and boundary conditions are shown in Fig. 5. Fig. 6 shows the detailed mesh around the initial crack tip.

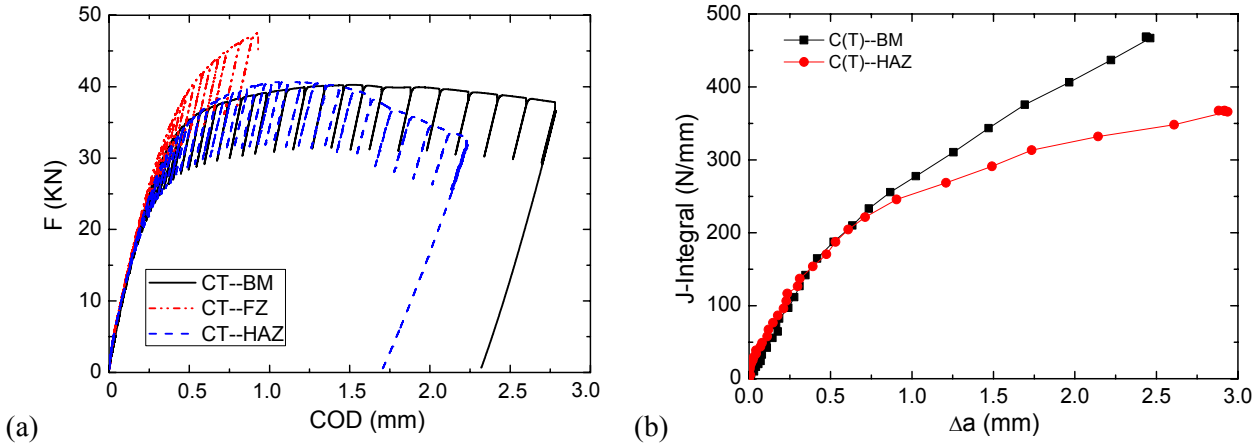

Fig. 2: Experimental (a) Force vs. Crack Opening Displacement (COD) and (b) fracture resistance J_R curves of compact tension (C(T)) specimens with the initial crack located in the BM, in the middle of the FZ and at the interface between the FZ and the HAZ, respectively.

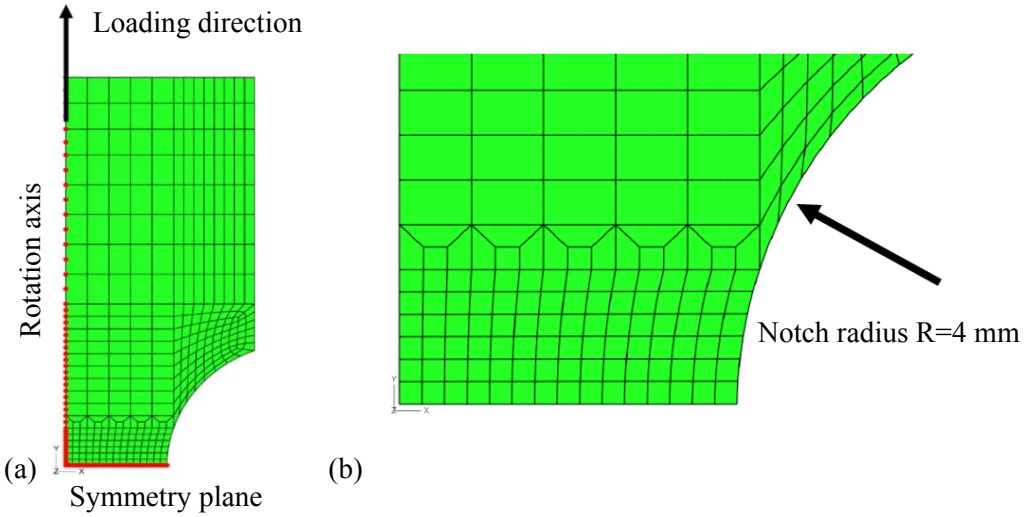

Fig. 3: (a) Axisymmetric finite element mesh and boundary conditions of the notched round specimen and (b) detailed mesh.

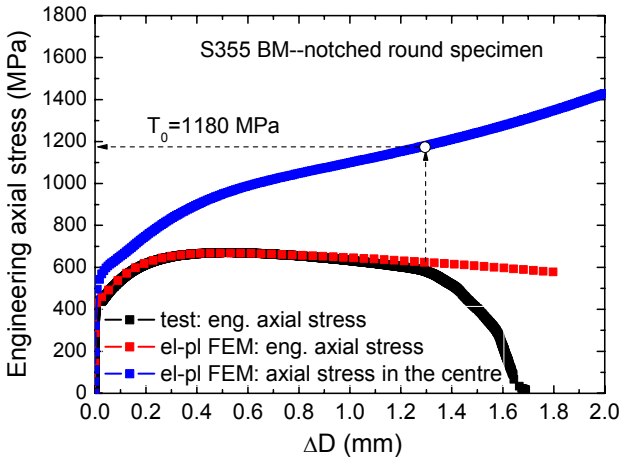

Fig. 4: Determination of the cohesive stress T_0: comparison of axial stress versus the diameter reduction curve from FE simulation and the experiments and the maximum true axial stress in the center of the specimen.

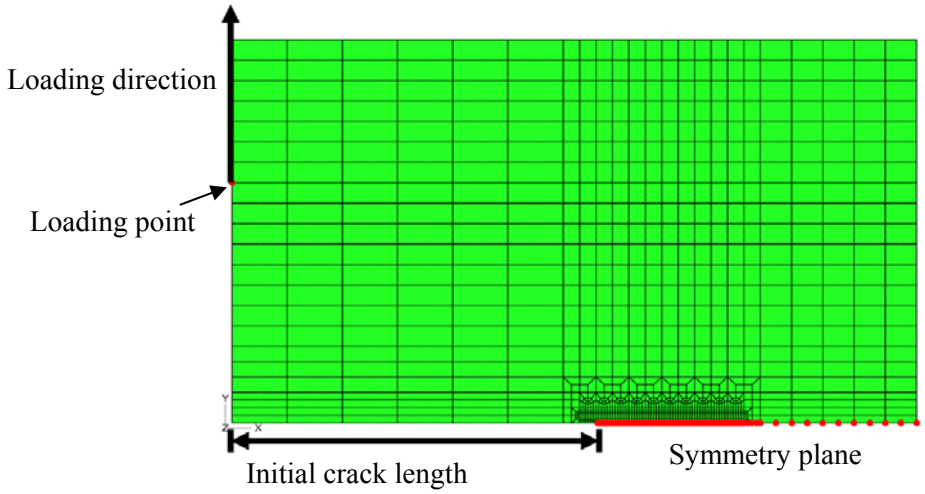

Fig. 5: Finite element mesh and boundary conditions of the C(T) specimen.

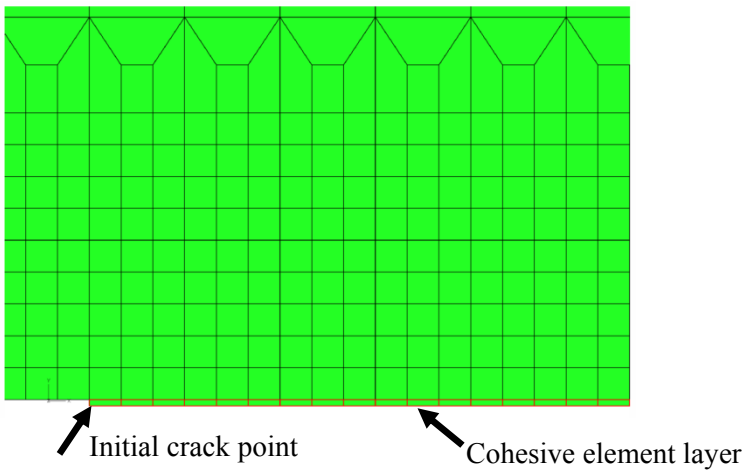

Fig. 6: Detailed finite element mesh around the initial crack position.

For the C(T)-BM specimen, when an exponential shape traction separation law is adopted, good agreement between the numerical and experimental results can be obtained in terms of FCOD and J_R curves when T_0=1180 MPa and Γ_0=18.5 N/mm are applied (Fig. 7). The trapezoid shape traction-separation law is also adopted to study the fracture behavior of the C(T)-BM specimen. As can be found in Fig. 8, good agreement between the numerical and experimental results can be obtained in terms of FCOD and J_R curves when T_0=1180 MPa and Γ_0=23.6 N/mm is used. This means that both exponential and trapezoid shape traction separation law can predict the crack propagation of C(T) specimens obtained from the BM well when different parameter sets are chosen.

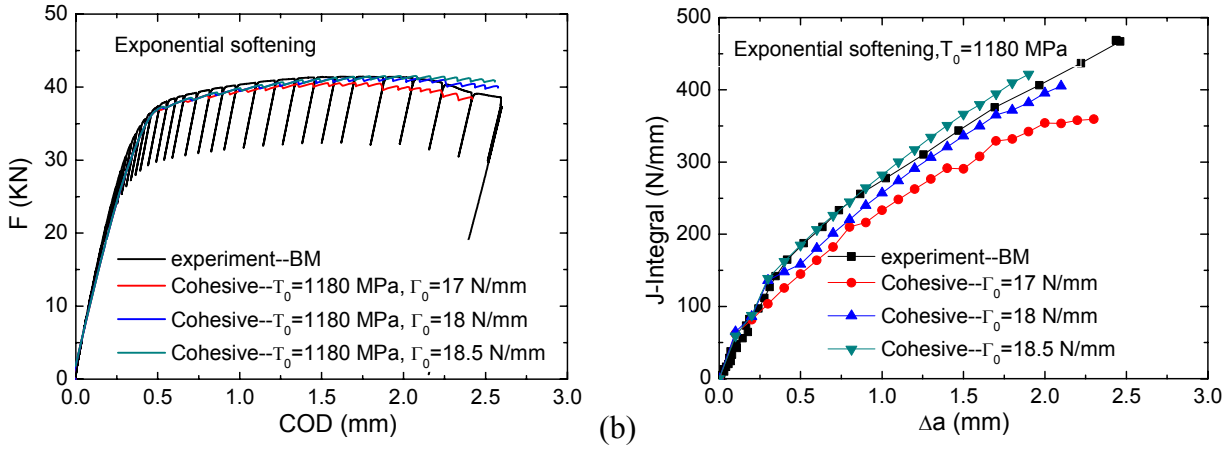

Fig. 7: Comparison of experimental and numerical (a) force vs. Crack Opening Displacement (COD) curves, and (b) fracture resistance curves for C(T) specimens with initial crack located in the BM when an exponential shape of the traction-separation law is adopted.

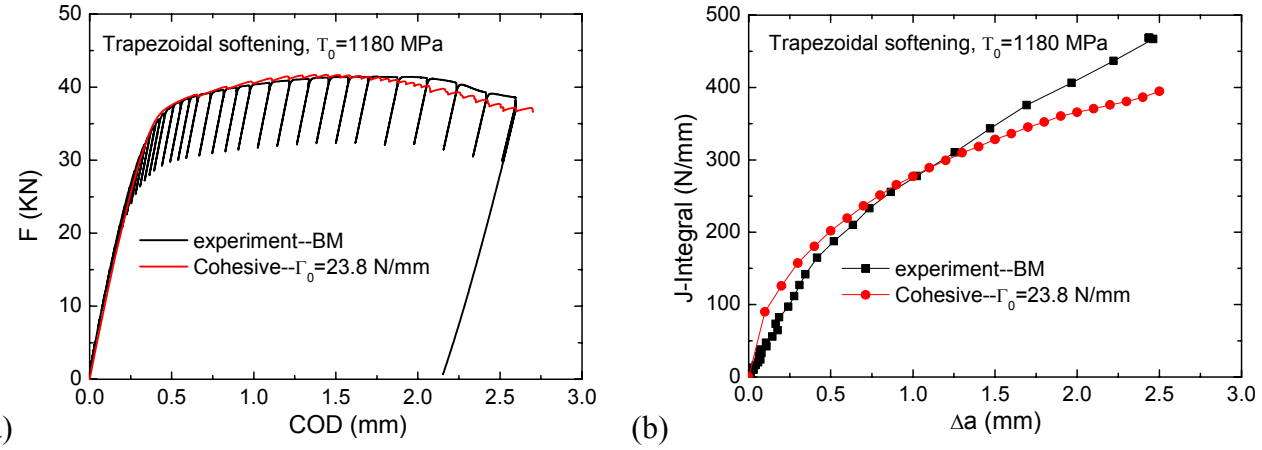

Fig. 8: Comparison of experimental and numerical (a) force vs. Crack Opening Displacement (COD) curves, and (b) fracture resistance curves for C(T) specimens with initial crack located in the BM when trapezoid shape traction separation law is adopted.

For the C(T)-FZ, as what has been observed in Fig. 2, the FZ showing more brittle behavior, a linear decreasing traction-separation law is required for the cohesive model. The numerical FCOD curve matches the experimental one well before the sudden rupture, showing the cohesive model

can predict the FCOD curve of the C(T)-FZ specimen well, as can be seen in Fig. 9. For the C(T)-HAZ specimen, an exponential traction-separation law is chosen for the cohesive model. Good agreement between the numerical and experimental results can be obtained in terms of FCOD and J_R curves when T_0=1350 MPa and Γ_0=16.5 N/mm is used, as can be found in Fig. 10.

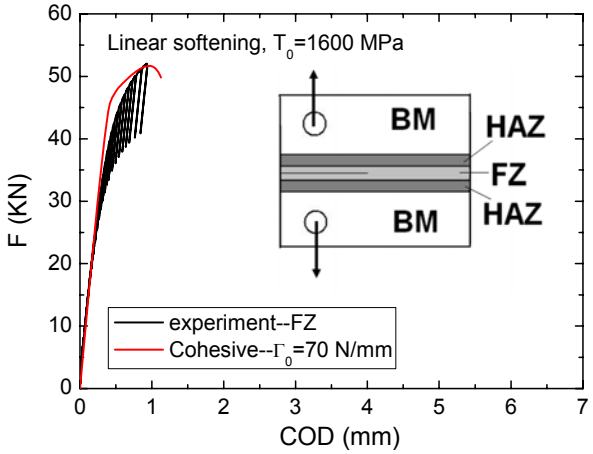

Fig. 9: Comparison of experimental and numerical force vs. Crack Opening Displacement (COD) curves for C(T) specimen with the initial crack located in the center of the FZ.

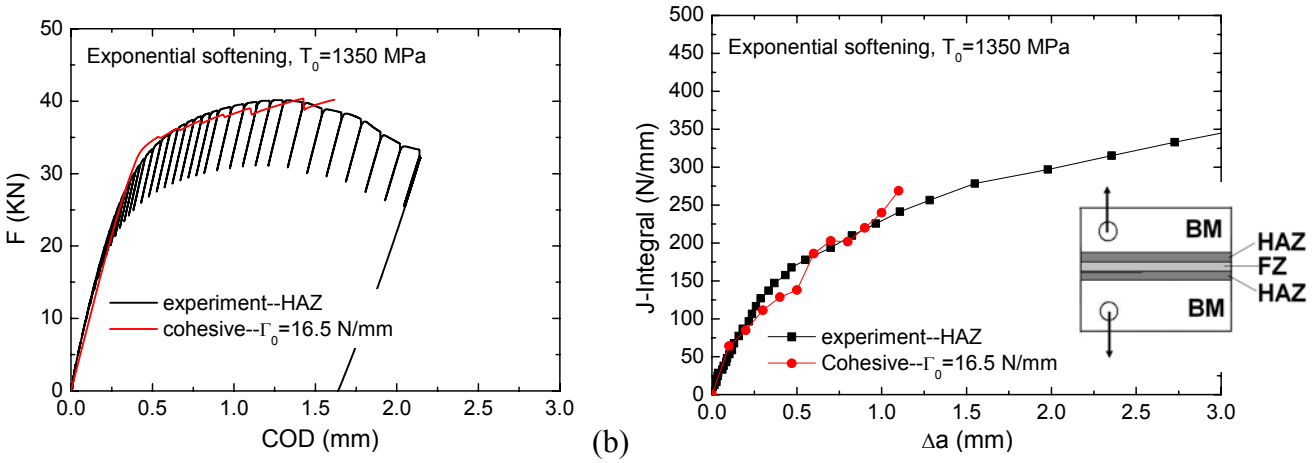

Fig. 10: Comparison of experimental and numerical (a) force vs. Crack Opening Displacement (COD) curves, and (b) fracture resistance curves for C(T) specimens with the initial crack located at the interface between the FZ and the HAZ when an exponential traction separation law is adopted.

4. Conclusions

Crack propagation was studied on S355 EBW joints using the cohesive model. Stress-strain curves of respective weld regions are derived from the tensile test results of flat specimens which are obtained from these regions. Three different C(T) specimens, i.e., the C(T)-BM, the C(T)-FZ and the C(T)-HAZ are investigated. Based on the axial stress versus diameter reduction curve of notched round specimens, the cohesive strength T_0 is fixed. When choosing different parameter sets for different traction separation laws, the cohesive model can predict the FCOD and J_R curve of C(T)

specimens from the BM well. This shows, both, exponential and trapezoid shaped traction-separation laws are able to predict the crack propagation in BM specimens. The cohesive model can also predict FCOD curves of C(T)-FZ specimens before the sudden rupture. When choosing the exponential traction-separation law, the cohesive model can predict good FCOD and J_R curve for the C(T)-HAZ specimens. All in all, the investigations of the fracture behavior of S355 EBW joints with the cohesive model confirm that the cohesive model is able to predict the crack propagation of the homogenous BM and the inhomogeneous welded joints well.

Acknowledgements

The research has been financially supported by China Scholarship Council (CSC) and SFB 716. This financial support is gratefully acknowledged. The authors would like to thank Prof. V. Ploshikhin and Dr. Y. Rudnik from Neue Materialien Bayreuth GmbH, for providing some of the experimental results.

Reference

[1] A. L. Gurson. Continuum theory of ductile rupture by void nucleation and growth: Part I-Yield criteria and flow rules for porous ductile media. J Eng Mater Techno-Trans. ASME 99 (1977), pp. 2-15.

[2] V. Tvergaard. Influence of void nucleation on ductile shear fracture at a free surface. J Mech Phys Solids 30 (1982), pp. 399-425.

[3] V. Tvergaard, A. Needleman. Analysis of the cup-cone fracture in a round tensile bar. Acta Metall 32 (1984), pp. 157-169.

[4] A. Needleman, V. Tvergaard. A micromechanical analysis of ductile-brittle transition at a weld. Engng Frac Mech 62 (1999), pp. 317-338.

[5] V. Tvergaard, A. Needleman. Analysis of the Charpy V-notch test for welds. Engng Frac Mech 65 (2000), pp. 627-643.

[6] V. Tvergaard, A. Needleman. 3D analyses of the effect of weld orientation in Charpy specimens. Engng Frac Mech 71 (2004), pp. 2179-2195.

[7] P. Nègre, D. Steglich, W. Brocks. Crack extension in aluminium welds: a numerical approach using the Gurson-Tvergaard-Needleman model. Engng Fract Mech 71 (2004), pp. 2365-2383.

[8] P. Nègre et al.. Numerical simulation of crack extension in aluminium welds. Comp Mater Sci 28 (2003), pp. 723-731.

[9] A. Nonn, W. Dahl, W. Bleck. Numerical modelling of damage behaviour of laser-hybrid welds. Engng Fract Mech 75 (2008), pp. 3251-3263.

[10] G. Rousselier. Ductile fracture models and their potential in local approach of fracture. Nucl Eng Design 105 (1987), pp. 97-111.

[11] H. Y. Tu, S. Schmauder, U. Weber, Y. Rudnik, V. Ploshikhin. Numerical simulation and experimental investigation of the damage behavior on electron beam welded joints. Proc Engng 10 (2011), pp. 875-880.

[12] H. Y. Tu, S. Schmauder, U. Weber, Y. Rudnik, V. Ploshikhin. Simulation of the damage behavior of electron beam welded joints with the Rousselier model. Engng Fract Mech (2012),

in press.

[13] H. Tu, S. Schmauder, U. Weber. Numerical study of electron beam welded butt joints with the GTN model. Comput Mech 50 (2012), pp. 245-255.

[14] D. S. Dugdale, Yielding of steel sheets containing slits. J Mech Phys Solids 8 (1960), pp. 100-104.

[15] G. I. Barenblatt. The mathematical theory of equilibrium cracks in brittle fracture. Adv Appl Mechanics 7 (1962), pp. 55-129.

[16] A. Hillerborg et al.. Analysis of crack formation and crack growth in concrete by means of fracture mechanics and finite elements. Cem Conc Research 6 (1976), pp. 773–782.

[17] A. Needleman. A continuum model for void nucleation by inclusion debonding. J Appl Mech ASME 54 (1987), pp. 525–531.

[18] A. Needleman. An analysis of decohesion along an imperfect interface. I J Frac 42 (1990), pp. 21-40.

[19] V. Tvergaard, J. W. Hutchinson. The relation between crack growth resistance and fracture process parameters in elastic-plastic solids. J Mech Phys Solids 40 (1992), pp. 1377–1397.

[20] I. Scheider. Bruchmechanische Bewertung von Laserschweissverbindungen durch numerische Rissfortschrittsimulation mit dem Kohäsivzonenmodell. PhD thesis, TU Hamburg-Harburg, Geesthacht, 2001.

[21] ASTM E 1820-96. Standard test method for measurement of fracture toughness. In: Annual Book of ASTM Standards, Vol. 03.01. American Society for Testing and Materials, Philadelphia, PA, USA.

[22] A. Cornec et al.. On the practical application of the cohesive model. Engng Fract Mech 70 (2003), pp. 1963-1987.